Volume 1 | Number 1 | Jan 2013 | Pages 1–100

Dalton Transactions

An international journal of inorganic chemistry
www.rsc.org/dalton

ROYAL SOCIETY OF CHEMISTRY

This is an *Accepted Manuscript*, which has been through the Royal Society of Chemistry peer review process and has been accepted for publication.

Accepted Manuscripts are published online shortly after acceptance, before technical editing, formatting and proof reading. Using this free service, authors can make their results available to the community, in citable form, before we publish the edited article. We will replace this *Accepted Manuscript* with the edited and formatted *Advance Article* as soon as it is available.

You can find more information about *Accepted Manuscripts* in the **Information for Authors**.

Please note that technical editing may introduce minor changes to the text and/or graphics, which may alter content. The journal's standard **Terms & Conditions** and the **Ethical guidelines** still apply. In no event shall the Royal Society of Chemistry be held responsible for any errors or omissions in this *Accepted Manuscript* or any consequences arising from the use of any information it contains.

Journal Name

ARTICLE

Thermodynamics of the structural transition in Metal-Organic Frameworks

J. Rodriguez[a], I. Beurroies[a], M.-V. Coulet[a], P. Fabry[b], T. Devic[b], C. Serre[b], R. Denoyel[a] and P. L. Llewellyn[a,*]

A thermodynamic study of the structural large-pore (LP) to narrow pore (NP) transition in various Metal Organic Frameworks (MOFs) is presented. First, the pressure induced transition at constant temperature is investigated using a Tian-Calvet microcalorimeter set-up equipped with a high pressure cell. This device permits simultaneous measurements of the mechanical work and heat associated to the LP→NP transition. It is shown that MIL-53(Al) and MIL-53(Cr) have similar thermodynamic and mechanical behaviour whilst the MIL-47(V) system is characterized by much higher transition energy and mechanical work. Second, the temperature induced transition at ambient pressure is studied by means of differential scanning calorimetry (DSC) combined with X-ray absorption spectroscopy. This set-up enables to follow simultaneously the structural changes associated with the phase transition detected by DSC. The MIL-53(Cr)-Br functionalized MOF is chosen here as a case study where both energetics and structural changes are discussed.

Introduction

Promising materials which induce easy and efficient mechanical energy storage are one of the challenging topics treated by numerous researchers today. Indeed, many applications, such as vehicle dampers, require ecological and efficient absorbers to dissipate the mechanical energy that is transmitted to the system by shocks or vibrations[1-4]. Mechanical systems can be classified as either shock absorbers (irreversible compression), dampers (compression-decompression with hysteresis) or molecular springs (compression-decompression without hysteresis)[5].

In recent decades, most of the attempts to use porous materials for such types of application were based on the forced wetting of hydrophobic materials. The considered systems are either mesoporous silica with a surface rendered hydrophobic via the grafting of hydrophobic functions, zeolites that are naturally hydrophobic such as silicalite[2,7] or more recently, porous coordination polymers such as ZIFs[8]. These systems have the property to accumulate, transform, restore or dissipate energy[9-12]. However, in many cases, colloidal damper performances are reported to decrease when the

number of working cycles increases. This may be due to changes in the pore structure as a result of the pressure cycles which will then alter the pore size distribution. One can also observe the appearance of hydrophilic patches resulting from the progressive rehydroxylation of the pore walls by water[6,12].

Metal Organic Frameworks (MOFs) are one of the recent classes of porous materials envisaged for damper applications. Indeed, the potential applications of MOFs are generally quoted in fields such as gas storage, separation of fluids, biomedicine and catalysis[13-17], however some MOFs were tested for their potential application as mechanical shock absorbers making use of their intrinsic flexibility. Here, the process is different from water intrusion/extrusion since the mechanical energy is not transformed into surface energy. Indeed the phenomenon used is the change of MOF structure from a large pore (LP) to a narrow pore (NP) form under the influence of pressure[18] leading to energy storage or dissipation. Experimentally, to study MOF compression-decompression, a non-penetrating fluid (i.e. which does not enter the porosity), often called a "pressurization media", is used to enable the structural transition of the material. MIL-53(Al), MIL-53(Cr) or MIL-47(V) are some of these MOFs able to perform a structural transition LP to NP forms, often reported as a "breathing behaviour" (MIL stands for Materials of Institut Lavoisier). These solids are built up from chains of corner-sharing oxy-metal octahedra connected by terephthalate ligands to define a diamond-shaped one-dimensional pore system of around 8.5 Å free diameter in the large pore form[18-22].

a. Aix-Marseille Université, CNRS, MADIREL-UMR 7246, Campus de St. Jérôme, 13397 Marseille cedex 20, France.
b. Institut Lavoisier Versailles, Université de Versailles St-Quentin, 45, avenue des Etats-Unis, 78035 Versailles cedex, France

This structural transition can be observed using mercury porosimetry that enables an isostatic pressure to be imposed around the MOF. The micropores of this material cannot be filled by mercury in the usual working pressure range, which means that apparent intrusion-extrusion volume of mercury relates directly to the MOF volume variation. By this method, the work related to the structural transition (*W*) may be derived[18, 23,24]. MOF mechanical energy storage performances are reported between 6.6 Jg^{-1} and 33 J g^{-1} with transition pressures in the range 18 MPa to 85 MPa. These results are in good agreement with typical values obtained for colloidal dampers in the order of 1-10 J g^{-1} with a compressive pressure in the range 20 MPa to 60 MPa[2,6,7]. It is worth noting that recent studies with hydrophobic materials using salt water leads to a large increase in intrusion pressure compared with pure water. This is due to the osmotic pressure effect resulting from the exclusion of ions from the pores. Energy storage performances around 30 J g^{-1} are thus obtained[17].

Heat measurements in this research field are rarely reported in the literature. Indeed, only a few articles report heat determination during intrusion/extrusion of water in hydrophobic nanopores [25-28] and only one article concerns MOF compression/ decompression[29]. Such measurements are essential as prior studies have shown that a temperature increase from 20°C to 100°C may result in the loss of fluid stability and component failure for magneto-rheological fluid dampers[30], an increase in damper stiffness[31], or an increase in the spring oscillation rate and in the static ride height [32]. One can thus appreciate that heat measurements are central to determine the complete thermodynamic properties of these systems. Indeed, there is an interest to determine the complete phase diagram of the flexible materials, *i.e.* P,V,T data in the largest range possible, coupled with values of transition energies to predict the thermal behaviour of practical systems. Due to the technical difficulties and also because materials of practical interest would be used close to ambient conditions, two complementary approaches are presented here. One is the determination of the transition energy when this transition is provoked by an external pressure change at constant temperature. The other is the determination of the transition energy when it is provoked by a temperature change at constant pressure. This is carried out using differential scanning calorimetry (DSC) where the heat released or absorbed by a sample is followed as a function of temperature. The first approach is useful to study MOF samples that are in the LP form at room temperature, whereas DSC is easier to use with samples that are in the NP form at room temperature. Moreover in this report, DSC is coupled with extended X-ray absorption spectroscopy (XAS) measurements to give simultaneous information about local structure. In this work, the structural transition, under the influence of pressure, of MIL-53(Al), MIL-53(Cr) and MIL-47(V) was studied whereas the transition under the influence of temperature at constant pressure was studied in the case of a Br-functionalized MIL-53(Cr) as the temperature of the transition NP to LP is more suited to the conditions employed. We show how the internal energy of the structural transition can be derived from mechanical work and heat measurements. Furthermore, by performing several thermodynamic cycles, it is possible to assess the aging of the materials.

For applications, mercury cannot be retained as a pressure transmission fluid for safety reasons and alternative fluids have been proposed including silicon oil[29], mineral oil[33], fluorinert[34] and 2-propanol[35] since they showed that they do not penetrate inside MOFs pores due to their size. Here, as an extension to previous work using a mixed water/oil system, we have developed a manifold using only silicon oil in which we are able perform the compression/depression cycles of the sample placed inside a calorimeter.

Materials and Methods

MOF Materials

Metal Organic Frameworks used for this work were synthesized following the reported procedures[36-38].

The first selected MOFs are the MIL-53(M^{3+}) and MIL-47(M^{4+}) systems which belong to the MIL series of hybrid porous materials. The MIL-53 and its isostructural form MIL-47, are built up from infinite chains of corner-sharing M^{3+}O$_4$(OH)$_2$ (M^{3+} = Al, Cr, Fe, Ga, Sc …) or M^{4+}O$_6$ (M^{4+} = V) octahedra interconnected by 1,4-benzenedicarboxylate groups[20,21]. Note that the MIL-53(Cr,Al) exhibits hydroxyl groups bridging the metal ions (μ_2-OH groups) which differ to that of MIL-47(V) where these groups are replaced by μ_2-O groups. In the LP form, these structures contain 1D diamond-shaped channels with pores of free diameter close to 8.5 Å. Finally, MIL-53(Cr) functionalized with bromide (denoted hereafter MIL-53(Cr)-Br) has been chosen to study the temperature induced NP→LP transition under constant pressure. This later was prepared following the reported conditions for MIL-53(Cr) by simply replacing the terephtahlic acid by bromoterephthalic acid. At ambient pressure, this sample adopts a NP form, which transit to a LP form between 107°C and 167°C[39]

High Pressure Calorimetry Experiments

The samples are activated directly in the high pressure (HP) cell. The activation step consists of heating the samples under secondary vacuum in order to evacuate residual adsorbed water molecules. The thermal treatment is carried out up to 250°C for MIL-53(Al), 210°C for MIL-53(Cr) and 170°C for MIL-47(V). After this step the MOFs studied are in the large pore (LP) form. The HP cell is then placed in the Tian-Calvet type microcalorimeter and attached to the high pressure intrusion set-up as shown in Fig. 1.

The manifold above the cell is then evacuated with a primary vacuum pump. After thermal equilibrium, the silicone oil (Silicone oil AP 100, Aldrich) is introduced to the whole system (manifold dosing volume and cell) up to a pressure of 2 MPa. The pressure is then increased in the cell step by step up to 250 MPa by injection of small, 30μL, volumes of oil to the system. After each injection, holding time of around one hour is maintained in order to reach thermal equilibrium in the

calorimetric signal. The injected volume, the equilibrium pressure and the heat evolved are measured for each step. The injected oil volume is thus measured as a function of pressure. After correction for the oil compressibility, and if we consider that the oil does not penetrate the porosity, this calculated volume variation corresponds to the variation of volume of the MOF.
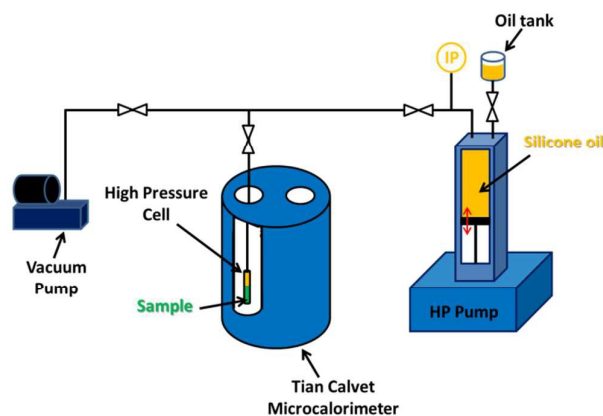

Fig. 1 Schematic representation of the high pressure calorimetry setup.

Similarly, the heat of compressibility of the silicone oil is evaluated by performing a blank experiment (without sample) which is then subtracted, considering the real volumes occupied by the oil and the solid, from the measurements made with sample in order to ascertain the heat corresponding to MOF structure transition. It is possible to calculate the transition internal energy variation by applying the first principle where the change in internal energy (U) is given by $\Delta U = Q + W$. Thus, the heat (Q) and the work (W) obtained during the compression-decompression of different MOFs such as MIL-53(Al), MIL-53(Cr) and MIL-47(V) are measured.

The work W provided to the system is obtained from the $P = f(V)$ data by integration, after subtraction of the oil compressibility:

$$W = -\int_A^B P dV \qquad (1)$$

The heat produced between A and B is calculated from the sum of heats at each pressure step after subtraction of the heat associated with the oil compressibility. In other words, the experimentally measured heat (Q_{exp}) is the sum of the heat of compressibility for the MOF (Q_W) and for the silicone oil (Q_{oil}).

$$Q_{exp} = Q_W + Q_{oil} \qquad (2)$$

Mercury Porosimetry

The MOF compressibility was also followed using mercury porosimetry. Mercury compression experiments were performed using an automated mercury intrusion porosimeter (Poremaster, Quantachrome instruments). Here again, the samples were activated under secondary vacuum prior to the

experiment using the outgassing temperatures mentioned above. The samples are transferred to the measurement cells in a glove box under argon. Then the experiment is carried out by first filling the cell with mercury up to 0.1 MPa before further filling up to 400 MPa.

Differential scanning calorimetry and X-ray absorption spectroscopy

Standard calorimetric measurements are performed using a Sensys heat-flux differential scanning calorimeter from Setaram. The experiments are performed under helium flow (30 mL min^{-1}) in order to ensure good heat conductivity and because helium adsorption onto MOFs is negligible. Experiments are performed either at 5°C min^{-1} or 10°C min^{-1} from ambient temperature up to 180°C. Systematically several cycles are performed and a 5 hours isotherm at 20°C is maintained between each cycle in order to ensure the complete reversibility of the phase transition. Sample activation is carried out *in-situ*, directly in the DSC during the first heating cycle. Open alumina sample pans are used with around 25 mg of sample. The exact quantity of sample (*i.e.* after water desorption) is evaluated by thermogravimetry analysis.

Combined DSC and X-ray absorption spectroscopy (XAS) experiments are also presented. The same calorimeter is used in its modified form as already described [40]. The combination of the techniques allows to follow precisely the structural changes associated to a phase transition. XAS experiments are realized on BM23 beamline at ESRF at the Br-edge (13.474 keV) using a Si(111) double crystal monochromator. The experiments are carried out in transmission geometry in quick-aquisition mode in order to collect one full spectrum very 30 s. The amount of sample is adjusted in order to optimize the absorption of the incident photon beam. Around 25mg of MIL-53(Cr)-Br is diluted into boron nitride powder. To ensure its homogeneity, the powder mixture is then gently milled for two minutes using vibrational ball milling. The resulting powder is compressed into a pellet. Finally, due to the limited beam time, it was not possible to perform 5 hours isotherms between the cycles.

Results and Discussion

Structural transition induced by pressure at constant temperature

The variations in the volumes of the MIL-53(Al,Cr) and MIL-47(V) samples as a function of the applied oil pressure are given in Figure 2. In each set of experiments, three to four cycles are shown. Absolute values of the volume variation are presented.

In each case, as the pressure is increased, there is a net decrease in MOF volume due to the large pore (LP) to narrow pore (NP) transition. As the pressure is subsequently decreased, the reverse transition (NP → LP) occurs at lower pressure leading to the observed hysteresis. The hysteresis

loops are characteristic of a damper behaviour which indicates the presence of an energetic barrier between the two phases[18]. However, whilst this transition seems quasi-reversible for the MIL-53(Cr) and MIL-47(V) over the cycles, there seems to be a loss of volume after the first cycle in the case of MIL-53(Al). This latter behaviour is the same as that previously observed with a slightly different oil-water experimental set-up [29].
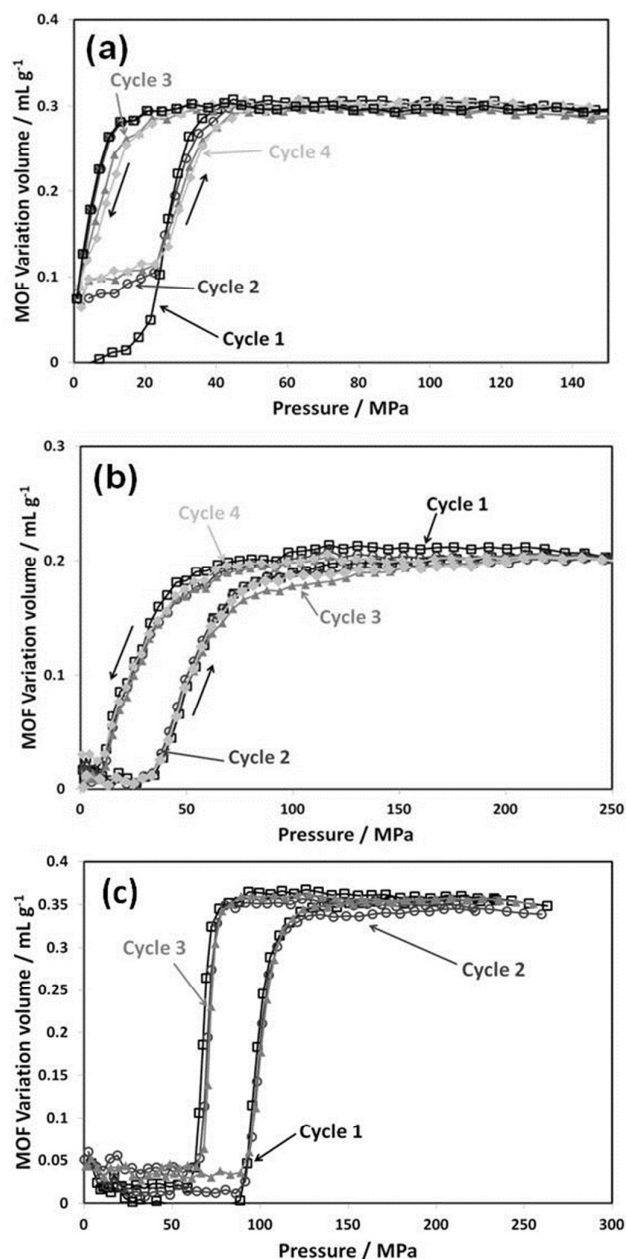

Fig. 2 System absolute volume variation as a function of the applied oil pressure in four compression/decompression cycles on MIL-53(Al) (a), MIL-53(Cr) (b) and MIL-47(V) (c) at 298K.

It can be of interest to compare the mechanical behaviour of these materials using various pressure transition media. Figure 3 shows a comparison between using silicone oil and mercury as pressure transmission media. For the systems shown, it can be seen that the volume variation of the MOFs are in the same range regardless the pressurization media.
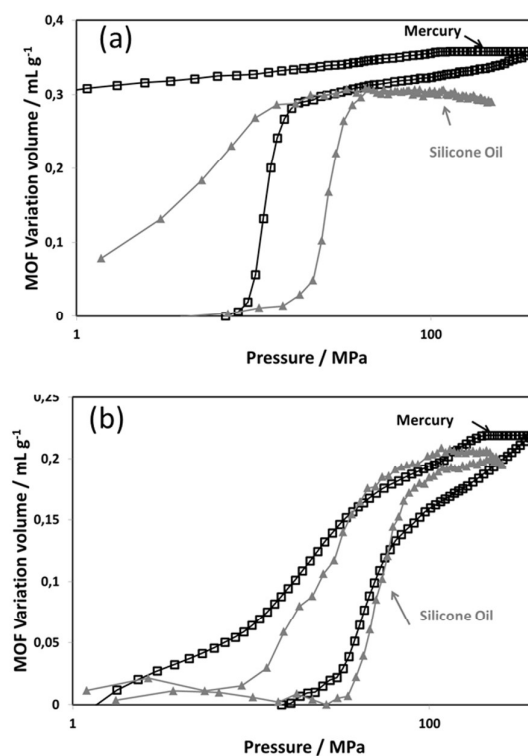

Fig. 3 MOF absolute volume variation during the first cycle as a function of the oil and mercury pressure on MIL-53(Al) (a) and MIL-53(Cr) (b) samples at 298K.

As previously observed[23,29] in the case of MIL-53(Al) the compression is irreversible using mercury porosimetry in contrast to what is observed with silicon oil. This can be interpreted by the possible partial penetration of the pore entrances by the chain ends of the oil molecules. This irreversibility in the case of mercury for MIL-53(Al) as compared to MIL-53(Cr) was explained [23] by strong π-π packing interactions between the phenyl rings (ligands) in the narrow pore structure of the MIL-53(Al). The narrow pore form of MIL-53(Cr) has indeed a slightly larger volume, which thus may lead to slightly lower π-π packing interactions and thus allow reopening of the structure at a higher pressure leading to a more reversible behaviour as observed in Figure 3.

Comparing the pressure at which the compression and decompression occur (Fig. 3 & Table 1), it can be observed that the transition occurs at a slightly higher pressure when using silicone oil in the case of MIL-53(Al). The same effect is observed with MIL-53(Cr) although less pronounced. It was hypothesised, as stated above, that the differences in transition pressure observed with the aluminium MOF could be due to partial penetration of the silicone oil chain in the MOF pores[29], the extent of this effect could be different

ARTICLE

between the two materials which present slight differences in pore size.

A notable difference relates to the pressure domain at which the transitions occur in the MIL-53(Al) system (100 MPA for mercury and 250 MPa for silicone oil). For MIL-53(Cr), differences also exists. With mercury, there is a sharp increase in the variation of MOF volume to approximately 0.15 mL g^{-1} up to 100 MPa, and then a slower continuous increase to 0.2 mL g^{-1} that occurs between 100 and 400 MPa. On the other hand, by using silicone oil, a sharp increase in the variation in MIL-53(Cr) volume to 0.2 mL g^{-1} occurs before 150 MPa with no further volume variation. These differences between the mercury and silicone oil results may also be due to the fact that mercury compression was a continuous one step process whilst silicone oil compression was performed step by step with lengthy equilibrium times. Indeed this kinetic difference in the sample compression may result in a slower and more efficient structural transition during the step by step (silicone oil) compression.

Table 1 MOF compression/decompression variation volumes and transition pressures using silicon oil and mercury as pressurization media.

MIL-	Silicon oil system			Hg porosimetry	
	53(Al)	53(Cr)	47(V)	53(Al)	53(Cr)
MOF variation volume (mL g^{-1})	0.3	0.2	0.35	0.3	0.2
Compression transition pressure (MPa)	20-40	35-90	86-134	13-18	20-110
Decompression transition pressure (MPa)	1-20	5-70	58-95	-	1-80

It is further possible to compare the variation in the volume of the MOFs using the different methods (Table 1). In both MIL-53 systems, equivalent volumes are observed whether silicone oil or mercury are used as pressurization media. One could expect a maximum volume variation of 35% if one considers the variation in crystallographic volumes (unit cell volume of the LP form ≈ 1424 Å^3, and of the NP form ≈ 920 Å^3 for MIL-53(Al)). These are equally similar to those observed previously[23,29]. In the case of MIL-53(Cr), whilst the transition pressures are in good agreement with previous results [18] the MOF variation volume is smaller (0.2 mL g^{-1}) than 0.25 mL g^{-1} obtained by *Beurroies et al.*[18] with mercury porosimetry. This difference is certainly due to the sample quality or activation.

Previous studies with MIL-47(V) using mercury as a pressure medium, show a volume variation of 0.45 mL g^{-1} and a transition pressure for the compression in the range 85-125 MPa [24]. Whilst the pressure range compares well with what is observed here with silicone oil, the variation in the volume observed is lower which we again attribute to differences in sample quality.

The energies measured during the compression and decompression are reported in Figure 4. The data are reported

per mass. For all the MOFs studied, the compression is accompanied by an exothermal effect, whilst the decompression is endothermic. Indeed, in all of our current work, this is the case. The heats measured before and after the transition are null within experimental error. It shows that the heat of compressibility of the NP and LP forms are small.

At this point, it is interesting to compare this energetic behaviour with alternative mechanical energy systems using water intrusion into hydrophobic porous media. Here, water intrusion can be accompanied by an exothermic effect with the siliceous form of the zeolite chabazite,[26] or with hydrophobic mesoporous silica[28]. However, with silicalite-1 [26] or ZIF-8 [27] an endothermic effect is observed with water intrusion. This endothermal effect is predicted by thermodynamics when wetting is reversible[41].

In the present case, we consider that there is no, or negligible, pore filling by the silicone oil. Thus, for flexible MOF materials, the competition between two energetic contributions, one due to the deformation of the bond angles and the other due to the distance between ligands, stabilizes one of the structural forms of the material (LP or NP)[18]. Considering these results, it is shown that structural transition from LP to NP was exothermic, while the transition from NP to LP was endothermic. As a consequence, MOF materials store mechanical energy and dissipate thermal energy, whereas, heterogeneous lyophobic systems with reversible intrusion-extrusion, store mechanical and thermal energy. This latter behaviour is interesting because it should prevent heating when the material is submitted to successive cycles.

The mechanical work (W) and measured energies (Q) are reported in Table 2. From these values it is possible to calculate the change in internal energy (U) during compression or decompression as well as the variation in internal energy during each cycle. With the exception of MIL-47(V), the heat of compression is in the same range as the mechanical work.

The mechanical work obtained for MIL-53(Al) is about 7.8 J g^{-1} during the first compression, then, it stabilizes around 6.0 J g^{-1} for the next three cycles. These results are in good agreement with the value previously reported of 6.6 J g^{-1} by mercury porosimetry [23]. Among the three MOFs studied here, this sample is the only one which provides a heat energy higher than the work energy, resulting in a negative compression internal energy (ΔU$_{comp.}$) about -2.5 J g^{-1} and a positive decompression internal energy (ΔU$_{decomp.}$) around 3.0 J g^{-1}. Again these observations correspond to those previously reported[29].

The compression work energy measured for MIL-53(Cr) stays constant during the four cycles at approximately 9.0 J g^{-1}, which is lower than that previously reported (~14 J g^{-1}). [18] This is simply a result of the lower variation in volume observed for the sample studied here.

In the case of MIL-47(V), *Yot et al.*[24] reported a mechanical compression work of 32.9 J g^{-1} and a mechanical decompression work of -19.5 J g^{-1} upon mercury porosimetry up to 350 MPa. As observed in Table 2, the silicone oil system leads to values of 34 J g^{-1} and -23 J g^{-1} for compression and

decompression respectively which are in good agreement with the reported values.
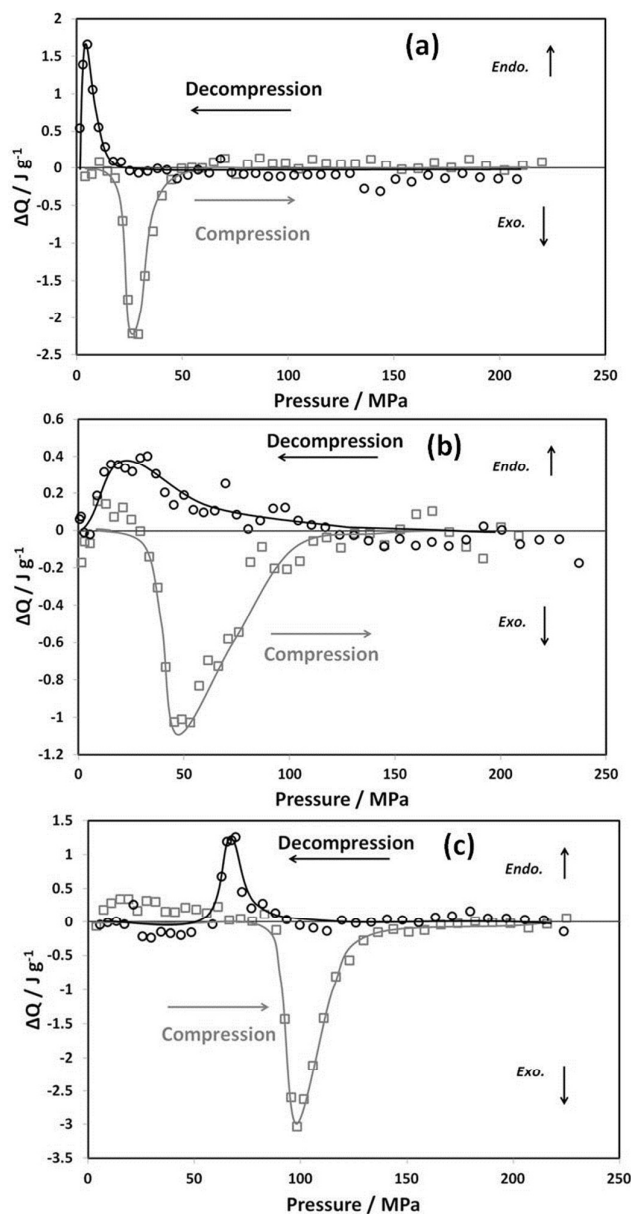

Fig. 4 Heat of compression and decompression as a function of the applied oil pressure for MIL-53(Al) (a), MIL-53(Cr) (b) and MIL-47(V) (c) at 298K during a cycle of compression/decompression.

It is possible to evaluate the overall heating of the samples during each cycle, i.e. ($Q_{comp.}$ + $Q_{decomp.}$). For the MIL-53 samples, this can be evaluated in the range -4 to -5 J g^{-1} per cycle, whereas this value reaches -8 to -10 J g^{-1} cycle^{-1} for MIL-47(V). This can be significant as in a real device, without effective heat management, an increase in temperature of several °C per cycle could occur.

When considering the change in internal energy for each cycle, a totally reversible process should give a value of zero. For the two MIL-53 samples, this is more or less the case when one

takes into consideration the experimental errors. However, for the MIL-47(V) system, a significant difference is observed. It may be possible to attribute this to a slow decrease in the work of compression with each cycle from 35.2 J g-1 to 33.1 J g-1, which could be due to a gradual degradation of the structure under the experimental conditions, this solid being knwon to be less stable than the MIL-53 counterparts

Structural transition induced by temperature at constant pressure

Fig. 5 represents the heat flow as a function of the temperature for the MIL-53(Cr)-Br sample under helium flow when heated at 5°Cmin^{-1} and 10°Cmin^{-1}.
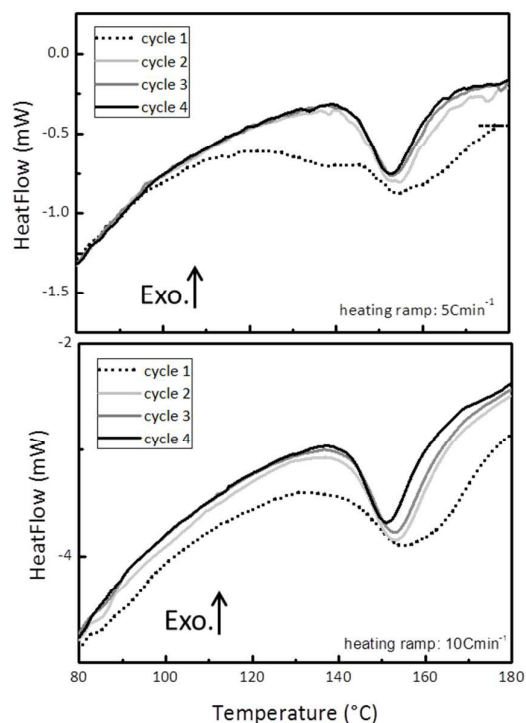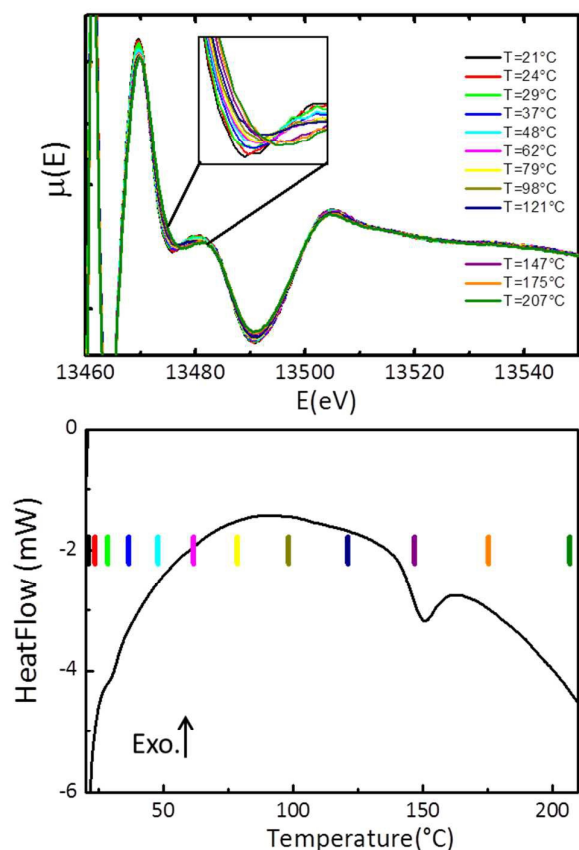

Fig. 5 DSC recording obtained at two different heating rates for MIL-53(Cr)-Br for successive cycles.

An endothermic peak is observed around 150°C and its width clearly decreases between the first cycle and the next ones. As previously explained, the sample is not activated prior to the DSC experiment. This means that, in its initial state, the sample contains residual water and has a NP structure. Thus during the first heating cycle two endothermic phenomena occur: water desorption and pore opening, which may explain the larger thermal effect.

During the following cycles, one may expect that only the structural NP→LP transition is observed. This assumption is confirmed by the XAS measurements. Indeed, as seen in Fig. 6, simultaneously to the transition observed by DSC, clear modifications in the XAS signal are evidenced. Those changes occur in the first 50eV after the absorption edge, the spectra are very sensitive to changes in the electronic structure around the absorbing atom. These changes are most probably related to a deviation in the local symmetry. Since the Br atoms are
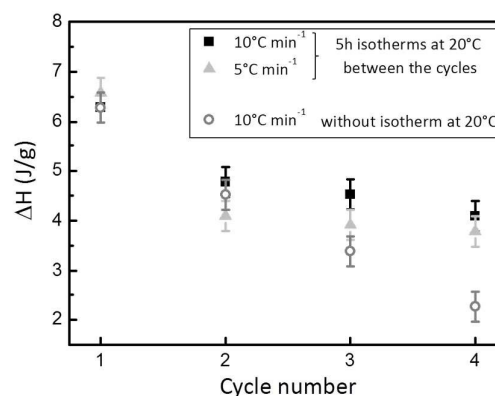
probed, this indicates that the pore opening is a collective mechanism which includes also changes in the periphery of the structure. A detailed structure analysis will be published elsewhere.

Fig. 6 (a) XAS spectra measured using the DSC-XAS setup for different temperatures. Note that to ensure legibility only every second spectrum is presented. (b) DSC recording performed at 10°C min⁻¹ and acquired simultaneously to the XAS spectra. The vertical markers correspond to the temperature at which the XAS signal were acquired (colour online)

Interestingly, the magnitude of the transition slowly decreases with an increase in the number of cycles (Fig. 7). This could be related (i) to kinetics: the transition LP→NP transition is slower that the NP→LP or (ii) to sample degradation at high temperature. In order to rule on those points, the enthalpy values are calculated for different heating programs and the obtained values are given in Fig.7. They are also compared to the renormalized enthalpy values obtained during the DSC-XAS experiment for which there was no isotherm step at ambient temperature. It is worth noting that, whatever the heating program, the enthalpy values slightly decrease as the number of cycles increases. The decay is faster when the cycles are performed without any isotherm step at ambient temperature. This suggests that the kinetics of the LP→NP transition are slower than the ones related to pore opening. One may note that the enthalpy values obtained at 10°C min⁻¹ are slightly

lower than the ones obtained at 5°C min⁻¹. This may indicate that the sample slowly degrades at high temperature since lower is the heating rate, longer the sample remains at high temperature.

Fig. 7 Enthalpy variation associated to the NP→LP transition as a function of the cycle number for MIL-53(Cr)-Br obtained under different heating programs.

Although the obtained enthalpy variations for the NP→LP transition cannot be compared to the corresponding internal energy variation since they were obtained at different temperatures, one may however observe that they are in the same range of around a few Joules per gram.

Conclusions

In summary, this thermodynamic study of MOFs describes how (i) to measure the heat and mechanical work during the structural transition between the LP form and the NP form at constant temperature enabling calculation of the internal energy and (ii) to determine the enthalpy of the transition under the influence of temperature at constant pressure. It is shown that these values are in the same range for the MIL-53(Al or Cr) series whereas larger energy variations are obtained for the MIL-47 sample. These results are of fundamental importance to determine the performances and the possible heating of these materials as dampers in practical applications.

From a practical point of view, the MIL-53(Al) and MIL-53(Cr) seem to possess equivalent performances in both heat and mechanical work. Nevertheless, they differ by their transition pressure which is higher for MIL-53(Cr) than for MIL-53(Al) (≈55 MPa versus ≈30 MPa). Otherwise, the MIL-47(V) outperforms the mechanical energy storage capacity of other MOFs which makes it a promising candidate for damper applications, despite a higher heating. However, its small loss of mechanical work capacity during the first three cycles may reveal degradation problems that should be confirmed in future studies. On the other hand, MIL-53 (Cr)-Br may not be used as damper at around ambient temperature. However its

property of opening under the influence of temperature could be applied to a use as actuator.

Table 2 Measured mechanical work and energy obtained for the compression and decompression cycles of samples and calculated internal energy changes associated with each step.

Cycle	MIL-53(Al)				MIL-53(Cr)				MIL-47(V)		
	1	2	3	4	1	2	3	4	1	2	3
$W_{comp.}$ (J g^{-1})	7.8	6.3	5.9	5.9	9.5	9.4	8.7	9.2	35.2	33.9	33.1
$Q_{comp.}$ (J g^{-1})	-9.9	-9.4	-8.7	-8.2	-9.1	-8.1	-7.8	-8.3	-15.6	-13.0	-12.9
$\Delta U_{comp.}$ (J g^{-1})	-2.1	-3.1	-2.8	-2.3	0.4	1.3	0.9	0.9	19.6	20.9	20.2
$W_{decomp.}$ (J g^{-1})	-	-1.7	-2.0	-2.1	-5.1	-5.4	-5.5	-5.0	-23.8	-22.0	-22.9
$Q_{decomp.}$ (J g^{-1})	-	5.7	4.5	4.9	4.1	4.5	4.7	4.7	5.2	4.8	4.9
$\Delta U_{decomp.}$ (J g^{-1})	-	4.0	2.5	2.8	-1.0	-0.9	-0.8	-0.3	-18.6	-17.2	-18.0
ΔU_{cycle} (J g^{-1})	-	0.9	-0.3	0.5	-0.6	0.3	0.1	0.6	1.0	3.7	2.2

Notes and references

1   J.-Q. Zhang, Z.-Z. Peng, L. Zhang and Y. Zhang, *Proceedings of the World Congress on Engineering*, 2013, **Vol. III**, WCE 2013, july 3 – 5 London, U. K .
2   C. V. Suciu, T. Iwatsubo, and S. Deki, *J. of coll. and inter. sci.*, 2003, **259**, 62-80.
3   S. K. Jha, *J. of Sound and Vibr.*, 1976, **47**, 543-558.
4   C. V. Suciu, *Proceedings of ISMA2010*, 2010, International Conference on Noise and Vibration Engineering (ISMA)/Conference of USD, Leuven, BELGIUM, 4233-4245.
5   B. Lefevre, A.Saugey, J. L. Barrat, L. Bocquet, E. Charlaix, P. F. Gobin and G. Vigier, *Coll. Surf. A*, 2004, **241**, 265-272.
6   C. V. Suciu and K. Yaguchi, *Exp. Mechanics*, 2009, **49**, 383-393.
7   Ya. Grosu, O. Ievtushenko, V. Eroshenko, J. M. Nedelec and J. P. E. Grolier, *Coll. Surf. A*, 2014, **441**, 54
8   Y. Grosu, V. Eroshenko, J. M. Nedelec and J. P. E. Grolier, *Phys. Chem. Chem. Phys.*, 2015, **17**, 1572.
9   L. Tzanis, H. Nouali, T. J. Daou, M. Soulard and J. Patarin, *Mater. Let.*, 2014, **115**, 229-232.
10 I. Khay, L. Tzanis, T. J. Daou, H. Nouali, A. Ryzhikov and J. Patarin, *Phys. Chem. Chem. Phys.*, 2013, **15**, 20320-20325.
11 M. A. Saada, S. Rigolet, J.-L. Paillaud, N. Bats, M. Soulard and J. Patarin, *J. Phys. Chem. C*, 2010, **114**, 11650-11658.
12 T. Karbowiak, C. Paulin, B. Ballandras, G. Weber, J.-P. Bellat *J. Am. Chem. Soc.*, 2009, **131**, 9898–9899.
13 G. Férey, *Chem. Soc. Rev.* 2008, **37**, 191-214.
14 G. Férey, C. Serre, T. Devic, G. Maurin, H. Jobic, P. L. Llewellyn, G. De Weireld, A. Vimont, M. Daturi and J. S. Chang, *Chem. Soc. Rev.*, 2011, **40**, 550-562.

15 J. Gascon, A. Corma, F. Kapteijn, and F. Llabrés i Xamena, *ACS Catal.*, 2014, **4**, 361-378.
16 P. Horcajada, R. Gref, T. Baati, P. K. Allan, G. Maurin, P. Couvreur, G. Férey, R. E. Morris and C. Serre, *Chem. Rev.*, 2011, **112**, 1232-1268
17 G. Ortiz, G. Chaplais, J.-L. Paillaud, H. Nouali, J. Patarin, J. Raya, and C. Marichal, *J. Phys. Chem. C*, 2014, **118**, 22021–22029
18 I. Beurroies, M. Boulhout, P. L. Llewellyn, B. Kuchta, G. Férey, C. Serre and R. Denoyel, *Angew. Chem., Int. Ed.*, 2010, **49**, 7526-7529.
19 T. Loiseau, C. Serre, C. Huguenard, G. Fink, F. Taulelle, M. Henry, T. Bataille and G. Férey, *Chem. Eur. J.*, 2004, **10**, 1373-
20 C. Serre, F. Millange, C. Thouvenot, M. Noguès, G. Marsolier, D. Louër and G. Férey, *J. Am. Chem. Soc.*, 2002, **124**, 13519-13526.
21   K. Barthelet, J. Marrot, D. Riou and G. Férey, *Angew. Chem. Int. Ed.*, 2002, **41**, 281-284.
22 E. Alvarez, N. Guillou, C. Martineau, B. Bueken, B. Van de Voorde, C. Le Guillouzer, P. Fabry, F. Nouar, F. Taulelle, D. de Vos, J.-S. Chang, K. H. Cho, N. Ramsahye, T. Devic, M. Daturi, G. Maurin and C. Serre, *Angew. Chem.*, 2015, **127**,1-6.
23 P. G. Yot, Z. Boudene, J. Macia, D. Granier, L. Vanduyfhuys, T. Verstraelen, V. Van Speybroeck, T. Devic, C. Serre, G. Férey, N. Stock, G. Maurin, *Chem. Comm.*, 2014, **50**, 9462-9464.
24 P. G. Yot, Q. Ma, J. Haines, Q. Yang, A. Ghoufi, T. Devic, C. Serre, V. Dmitriec, G. Férey, C. Zhong and G. Maurin, *Chem. Sci.*, 2012, **3**, 1100-1104.
25 T. Karbowiak, C. Paulin and J.-P. Bellat, *Microp. And Masop. Mater.*, 2010, **134**, 8-15.
26 T. Karbowiak, G. Weber and J.-P. Bellat, *Langmuir*, 2014, **30**, 213-219.
27 Ya. Grosu, G. Renaudin, V. Eroshenko, J.- M. Nedelec and J.-P. E. Grolier, *Nanoscale*, 2015, **7**, 8803–8810.
28 F. Gomez, R. Denoyel and J. Rouquerol, *Langmuir*, 2000, 16, 4374-4379.
29 J. Rodriguez, I. Beurroies, T. Loiseau, R. Denoyel and P. L. Llewellyn, *Angew. Chem., Int. Ed.*, 2015, **54**, 4626-4630.
30 M. B. Dogruoz, E. L. Wang, F. Gordaninejad, A, J. Stipanovic, *J. of Intel. Mater. Syst. and Struc.*, 2003, **14**, 79-86.
31 D. Bartterbee and D. Sims, *J. of Intel. Mater. Syst. And Struct.*, 2009, **20**, 297-309.

32 P. S. Els, B. Grobbelaar, *J. of Terramechanics*, 1999, **36**, 197-205.

33 P. Serra-Crespo, A. Dikhtiarenko, E. Stavitski, J. Juan-Alcañiz, F. Kapteijn, F.-X. Coudert and J. Gascon, *CrystEngComm*, 2015, **17**, 276-280.

34 K. W. Chapman, G. J. Halder and P. J. Chapus, *J. Amer. Chem. Soc*., 2009, **131**, 17546-17547.

35 E. C. Spencer, R. J. Angel, N. L. Ross, B. E. Hanson, J. A. K. Howard, *J. Amer. Chem. Soc*., 2009, **131**, 4022-4026.

36 C. Serre F. Millange , C. Thouvenot , M. Noguès , G. Marsolier, D. Louër and G. Férey, *J. Am. Chem. Soc.*, 2002, **124**, 13519–13526.

37 T. Loiseau, C. Serre, C. Huguenard, G. Fink, F. Taulelle, M. Henry,T. Bataille and G. Férey, *Chem. Eur. J.* 2004, **10**, 1373-1382.

38 K. Barthelet, J. Marrot, D. Riou and G. Férey, *Angew. Chem. Int. Ed.* 2002, **41**, 281-284.

39 V. Guillerm, 2011, Synthèse, fonctionnalisation et propriétés d'adsorption de nouveaux solides hybrides poreux, PhD Thesis, Université de Versailles.

40 P. Zalden, G. Aquilanti, C. Prestipino, O. Mathon, B. André, M. Wuttig, M.-V. Coulet, *J. Synchrotron Rad.*, 2012, **19**, 806-813.

41 Eroshenko, V. A., *Proc. of Institution Mechanical Engineers Part D*, 2007*, **221**, 285-300.

Journal Name

ARTICLE

Thermodynamics of the structural transition in Metal-Organic Frameworks

J. Rodriguez[a], I. Beurroies[a], M.-V. Coulet[a], P. Fabry[b], T. Devic[b], C. Serre[b], R. Denoyel[a] and P. L. Llewellyn[a,*]

A thermodynamic study of the structural large-pore (LP) to narrow pore (NP) transition in various Metal Organic Frameworks (MOFs) is presented. First, the pressure induced transition at constant temperature is investigated using a Tian-Calvet microcalorimeter set-up equipped with a high pressure cell. This device permits simultaneous measurements of the mechanical work and heat associated to the LP→NP transition. It is shown that MIL-53(Al) and MIL-53(Cr) have similar thermodynamic and mechanical behaviour whilst the MIL-47(V) system is characterized by much higher transition energy and mechanical work. Second, the temperature induced transition at ambient pressure is studied by means of differential scanning calorimetry (DSC) combined with X-ray absorption spectroscopy. This set-up enables to follow simultaneously the structural changes associated with the phase transition detected by DSC. The MIL-53(Cr)-Br functionalized MOF is chosen here as a case study where both energetics and structural changes are discussed.

Introduction

Promising materials which induce easy and efficient mechanical energy storage are one of the challenging topics treated by numerous researchers today. Indeed, many applications, such as vehicle dampers, require ecological and efficient absorbers to dissipate the mechanical energy that is transmitted to the system by shocks or vibrations[1-4]. Mechanical systems can be classified as either shock absorbers (irreversible compression), dampers (compression-decompression with hysteresis) or molecular springs (compression-decompression without hysteresis)[5].

In recent decades, most of the attempts to use porous materials for such types of application were based on the forced wetting of hydrophobic materials. The considered systems are either mesoporous silica with a surface rendered hydrophobic via the grafting of hydrophobic functions, zeolites that are naturally hydrophobic such as silicalite[2,7] or more recently, porous coordination polymers such as ZIFs[8]. These systems have the property to accumulate, transform, restore or dissipate energy[9-12]. However, in many cases, colloidal damper performances are reported to decrease when the

number of working cycles increases. This may be due to changes in the pore structure as a result of the pressure cycles which will then alter the pore size distribution. One can also observe the appearance of hydrophilic patches resulting from the progressive rehydroxylation of the pore walls by water[6,12].

Metal Organic Frameworks (MOFs) are one of the recent classes of porous materials envisaged for damper applications. Indeed, the potential applications of MOFs are generally quoted in fields such as gas storage, separation of fluids, biomedicine and catalysis[13-17], however some MOFs were tested for their potential application as mechanical shock absorbers making use of their intrinsic flexibility. Here, the process is different from water intrusion/extrusion since the mechanical energy is not transformed into surface energy. Indeed the phenomenon used is the change of MOF structure from a large pore (LP) to a narrow pore (NP) form under the influence of pressure[18] leading to energy storage or dissipation. Experimentally, to study MOF compression-decompression, a non-penetrating fluid (i.e. which does not enter the porosity), often called a "pressurization media", is used to enable the structural transition of the material. MIL-53(Al), MIL-53(Cr) or MIL-47(V) are some of these MOFs able to perform a structural transition LP to NP forms, often reported as a "breathing behaviour" (MIL stands for Materials of Institut Lavoisier). These solids are built up from chains of corner-sharing oxy-metal octahedra connected by terephthalate ligands to define a diamond-shaped one-dimensional pore system of around 8.5 Å free diameter in the large pore form[18-22].

a. Aix-Marseille Université, CNRS, MADIREL-UMR 7246, Campus de St. Jérôme, 13397 Marseille cedex 20, France.
b. Institut Lavoisier Versailles, Université de Versailles St-Quentin, 45, avenue des Etats-Unis, 78035 Versailles cedex, France
† Footnotes relating to the title and/or authors should appear here.
Electronic Supplementary Information (ESI) available: [details of any supplementary information available should be included here]. See DOI: 10.1039/x0xx00000x

Dalton Transactions Accepted Manuscript

This structural transition can be observed using mercury porosimetry that enables an isostatic pressure to be imposed around the MOF. The micropores of this material cannot be filled by mercury in the usual working pressure range, which means that apparent intrusion-extrusion volume of mercury relates directly to the MOF volume variation. By this method, the work related to the structural transition (*W*) may be derived[18, 23,24]. MOF mechanical energy storage performances are reported between 6.6 Jg^{-1} and 33 J g^{-1} with transition pressures in the range 18 MPa to 85 MPa. These results are in good agreement with typical values obtained for colloidal dampers in the order of 1-10 J g^{-1} with a compressive pressure in the range 20 MPa to 60 MPa[2,6,7]. It is worth noting that recent studies with hydrophobic materials using salt water leads to a large increase in intrusion pressure compared with pure water. This is due to the osmotic pressure effect resulting from the exclusion of ions from the pores. Energy storage performances around 30 J g^{-1} are thus obtained[17].

Heat measurements in this research field are rarely reported in the literature. Indeed, only a few articles report heat determination during intrusion/extrusion of water in hydrophobic nanopores [25-28] and only one article concerns MOF compression/ decompression[29]. Such measurements are essential as prior studies have shown that a temperature increase from 20°C to 100°C may result in the loss of fluid stability and component failure for magneto-rheological fluid dampers[30], an increase in damper stiffness[31], or an increase in the spring oscillation rate and in the static ride height [32]. One can thus appreciate that heat measurements are central to determine the complete thermodynamic properties of these systems. Indeed, there is an interest to determine the complete phase diagram of the flexible materials, *i.e.* P,V,T data in the largest range possible, coupled with values of transition energies to predict the thermal behaviour of practical systems. Due to the technical difficulties and also because materials of practical interest would be used close to ambient conditions, two complementary approaches are presented here. One is the determination of the transition energy when this transition is provoked by an external pressure change at constant temperature. The other is the determination of the transition energy when it is provoked by a temperature change at constant pressure. This is carried out using differential scanning calorimetry (DSC) where the heat released or absorbed by a sample is followed as a function of temperature. The first approach is useful to study MOF samples that are in the LP form at room temperature, whereas DSC is easier to use with samples that are in the NP form at room temperature. Moreover in this report, DSC is coupled with extended X-ray absorption spectroscopy (XAS) measurements to give simultaneous information about local structure. In this work, the structural transition, under the influence of pressure, of MIL-53(Al), MIL-53(Cr) and MIL-47(V) was studied whereas the transition under the influence of temperature at constant pressure was studied in the case of a Br-functionalized MIL-53(Cr) as the temperature of the transition NP to LP is more suited to the conditions employed. We show how the internal energy of the structural transition

can be derived from mechanical work and heat measurements. Furthermore, by performing several thermodynamic cycles, it is possible to assess the aging of the materials.

For applications, mercury cannot be retained as a pressure transmission fluid for safety reasons and alternative fluids have been proposed including silicon oil[29], mineral oil[33], fluorinert[34] and 2-propanol[35] since they showed that they do not penetrate inside MOFs pores due to their size. Here, as an extension to previous work using a mixed water/oil system, we have developed a manifold using only silicon oil in which we are able perform the compression/depression cycles of the sample placed inside a calorimeter.

Materials and Methods

MOF Materials

Metal Organic Frameworks used for this work were synthesized following the reported procedures[36-38].

The first selected MOFs are the MIL-53(M^{3+}) and MIL-47(M^{4+}) systems which belong to the MIL series of hybrid porous materials. The MIL-53 and its isostructural form MIL-47, are built up from infinite chains of corner-sharing M^{3+}O$_4$(OH)$_2$ (M^{3+} = Al, Cr, Fe, Ga, Sc …) or M^{4+}O$_6$ (M^{4+} = V) octahedra interconnected by 1,4-benzenedicarboxylate groups[20,21]. Note that the MIL-53(Cr,Al) exhibits hydroxyl groups bridging the metal ions (μ_2-OH groups) which differ to that of MIL-47(V) where these groups are replaced by μ_2-O groups. In the LP form, these structures contain 1D diamond-shaped channels with pores of free diameter close to 8.5 Å. Finally, MIL-53(Cr) functionalized with bromide (denoted hereafter MIL-53(Cr)-Br) has been chosen to study the temperature induced NP→LP transition under constant pressure. This later was prepared following the reported conditions for MIL-53(Cr) by simply replacing the terephtahlic acid by bromoterephthalic acid. At ambient pressure, this sample adopts a NP form, which transit to a LP form between 107°C and 167°C[39]

High Pressure Calorimetry Experiments

The samples are activated directly in the high pressure (HP) cell. The activation step consists of heating the samples under secondary vacuum in order to evacuate residual adsorbed water molecules. The thermal treatment is carried out up to 250°C for MIL-53(Al), 210°C for MIL-53(Cr) and 170°C for MIL-47(V). After this step the MOFs studied are in the large pore (LP) form. The HP cell is then placed in the Tian-Calvet type microcalorimeter and attached to the high pressure intrusion set-up as shown in Fig. 1.

The manifold above the cell is then evacuated with a primary vacuum pump. After thermal equilibrium, the silicone oil (Silicone oil AP 100, Aldrich) is introduced to the whole system (manifold dosing volume and cell) up to a pressure of 2 MPa. The pressure is then increased in the cell step by step up to 250 MPa by injection of small, 30μL, volumes of oil to the system. After each injection, holding time of around one hour is maintained in order to reach thermal equilibrium in the

calorimetric signal. The injected volume, the equilibrium pressure and the heat evolved are measured for each step. The injected oil volume is thus measured as a function of pressure. After correction for the oil compressibility, and if we consider that the oil does not penetrate the porosity, this calculated volume variation corresponds to the variation of volume of the MOF.
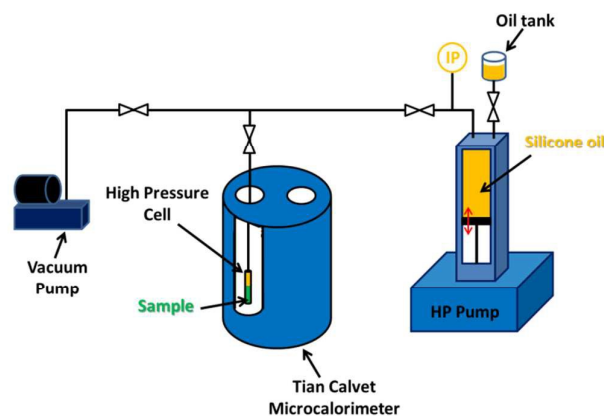

Fig. 1 Schematic representation of the high pressure calorimetry setup.

Similarly, the heat of compressibility of the silicone oil is evaluated by performing a blank experiment (without sample) which is then subtracted, considering the real volumes occupied by the oil and the solid, from the measurements made with sample in order to ascertain the heat corresponding to MOF structure transition. It is possible to calculate the transition internal energy variation by applying the first principle where the change in internal energy (U) is given by $\Delta U = Q + W$. Thus, the heat (Q) and the work (W) obtained during the compression-decompression of different MOFs such as MIL-53(Al), MIL-53(Cr) and MIL-47(V) are measured.

The work W provided to the system is obtained from the $P = f(V)$ data by integration, after subtraction of the oil compressibility:

$$W = -\int_A^B P dV \qquad (1)$$

The heat produced between A and B is calculated from the sum of heats at each pressure step after subtraction of the heat associated with the oil compressibility. In other words, the experimentally measured heat (Q_{exp}) is the sum of the heat of compressibility for the MOF (Q_W) and for the silicone oil (Q_{oil}).

$$Q_{exp} = Q_W + Q_{oil} \qquad (2)$$

Mercury Porosimetry

The MOF compressibility was also followed using mercury porosimetry. Mercury compression experiments were performed using an automated mercury intrusion porosimeter (Poremaster, Quantachrome instruments). Here again, the samples were activated under secondary vacuum prior to the

experiment using the outgassing temperatures mentioned above. The samples are transferred to the measurement cells in a glove box under argon. Then the experiment is carried out by first filling the cell with mercury up to 0.1 MPa before further filling up to 400 MPa.

Differential scanning calorimetry and X-ray absorption spectroscopy

Standard calorimetric measurements are performed using a Sensys heat-flux differential scanning calorimeter from Setaram. The experiments are performed under helium flow (30 mL min⁻¹) in order to ensure good heat conductivity and because helium adsorption onto MOFs is negligible. Experiments are performed either at 5°C min⁻¹ or 10°C min⁻¹ from ambient temperature up to 180°C. Systematically several cycles are performed and a 5 hours isotherm at 20°C is maintained between each cycle in order to ensure the complete reversibility of the phase transition. Sample activation is carried out *in-situ*, directly in the DSC during the first heating cycle. Open alumina sample pans are used with around 25 mg of sample. The exact quantity of sample (*i.e.* after water desorption) is evaluated by thermogravimetry analysis.

Combined DSC and X-ray absorption spectroscopy (XAS) experiments are also presented. The same calorimeter is used in its modified form as already described [40]. The combination of the techniques allows to follow precisely the structural changes associated to a phase transition. XAS experiments are realized on BM23 beamline at ESRF at the Br-edge (13.474 keV) using a Si(111) double crystal monochromator. The experiments are carried out in transmission geometry in quick-aquisition mode in order to collect one full spectrum very 30 s. The amount of sample is adjusted in order to optimize the absorption of the incident photon beam. Around 25mg of MIL-53(Cr)-Br is diluted into boron nitride powder. To ensure its homogeneity, the powder mixture is then gently milled for two minutes using vibrational ball milling. The resulting powder is compressed into a pellet. Finally, due to the limited beam time, it was not possible to perform 5 hours isotherms between the cycles.

Results and Discussion

Structural transition induced by pressure at constant temperature

The variations in the volumes of the MIL-53(Al,Cr) and MIL-47(V) samples as a function of the applied oil pressure are given in Figure 2. In each set of experiments, three to four cycles are shown. Absolute values of the volume variation are presented.

In each case, as the pressure is increased, there is a net decrease in MOF volume due to the large pore (LP) to narrow pore (NP) transition. As the pressure is subsequently decreased, the reverse transition (NP → LP) occurs at lower pressure leading to the observed hysteresis. The hysteresis

loops are characteristic of a damper behaviour which indicates the presence of an energetic barrier between the two phases[18]. However, whilst this transition seems quasi-reversible for the MIL-53(Cr) and MIL-47(V) over the cycles, there seems to be a loss of volume after the first cycle in the case of MIL-53(Al). This latter behaviour is the same as that previously observed with a slightly different oil-water experimental set-up [29].
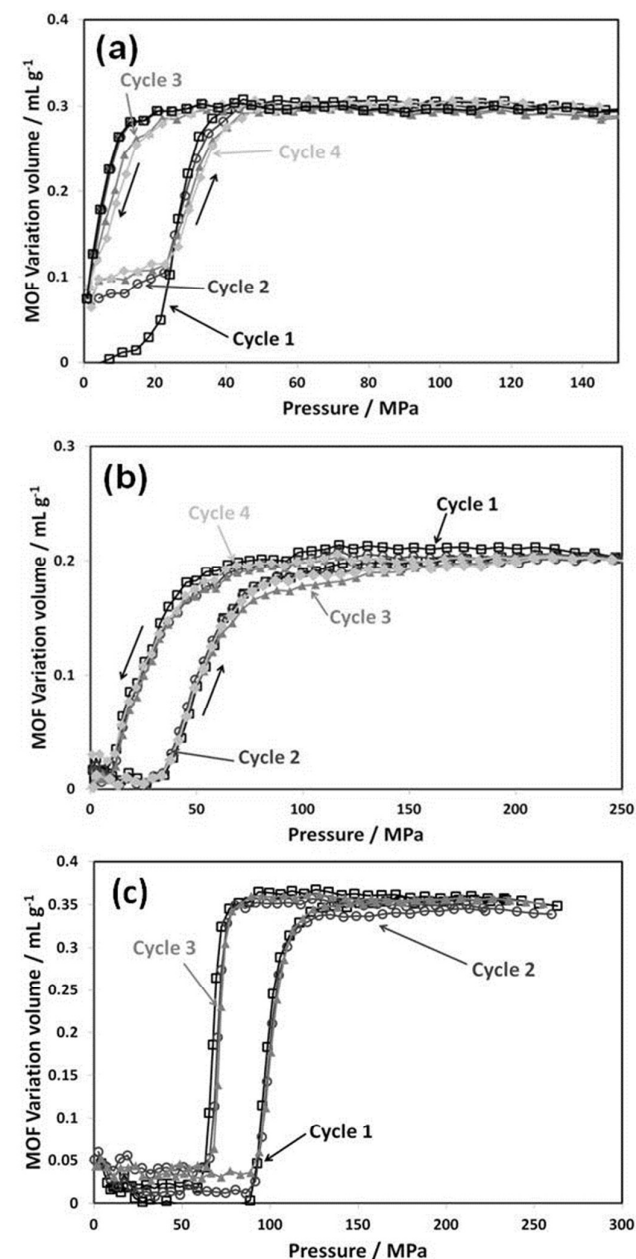

Fig. 2 System absolute volume variation as a function of the applied oil pressure in four compression/decompression cycles on MIL-53(Al) (a), MIL-53(Cr) (b) and MIL-47(V) (c) at 298K.

It can be of interest to compare the mechanical behaviour of these materials using various pressure transition media. Figure 3 shows a comparison between using silicone oil and mercury as pressure transmission media. For the systems shown, it can be seen that the volume variation of the MOFs are in the same range regardless the pressurization media.
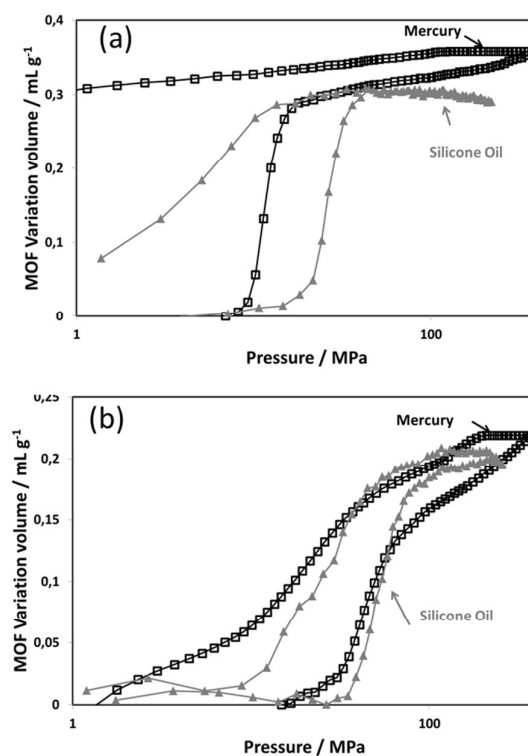

Fig. 3 MOF absolute volume variation during the first cycle as a function of the oil and mercury pressure on MIL-53(Al) (a) and MIL-53(Cr) (b) samples at 298K.

As previously observed[23,29] in the case of MIL-53(Al) the compression is irreversible using mercury porosimetry in contrast to what is observed with silicon oil. This can be interpreted by the possible partial penetration of the pore entrances by the chain ends of the oil molecules. This irreversibility in the case of mercury for MIL-53(Al) as compared to MIL-53(Cr) was explained [23] by strong π-π packing interactions between the phenyl rings (ligands) in the narrow pore structure of the MIL-53(Al). The narrow pore form of MIL-53(Cr) has indeed a slightly larger volume, which thus may lead to slightly lower π-π packing interactions and thus allow reopening of the structure at a higher pressure leading to a more reversible behaviour as observed in Figure 3.

Comparing the pressure at which the compression and decompression occur (Fig. 3 & Table 1), it can be observed that the transition occurs at a slightly higher pressure when using silicone oil in the case of MIL-53(Al). The same effect is observed with MIL-53(Cr) although less pronounced. It was hypothesised, as stated above, that the differences in transition pressure observed with the aluminium MOF could be due to partial penetration of the silicone oil chain in the MOF pores[29], the extent of this effect could be different

between the two materials which present slight differences in pore size.

A notable difference relates to the pressure domain at which the transitions occur in the MIL-53(Al) system (100 MPA for mercury and 250 MPa for silicone oil). For MIL-53(Cr), differences also exists. With mercury, there is a sharp increase in the variation of MOF volume to approximately 0.15 mL g^{-1} up to 100 MPa, and then a slower continuous increase to 0.2 mL g^{-1} that occurs between 100 and 400 MPa. On the other hand, by using silicone oil, a sharp increase in the variation in MIL-53(Cr) volume to 0.2 mL g^{-1} occurs before 150 MPa with no further volume variation. These differences between the mercury and silicone oil results may also be due to the fact that mercury compression was a continuous one step process whilst silicone oil compression was performed step by step with lengthy equilibrium times. Indeed this kinetic difference in the sample compression may result in a slower and more efficient structural transition during the step by step (silicone oil) compression.

Table 1 MOF compression/decompression variation volumes and transition pressures using silicon oil and mercury as pressurization media.

MIL-	Silicon oil system			Hg porosimetry	
	53(Al)	53(Cr)	47(V)	53(Al)	53(Cr)
MOF variation volume (mL g^{-1})	0.3	0.2	0.35	0.3	0.2
Compression transition pressure (MPa)	20-40	35-90	86-134	13-18	20-110
Decompression transition pressure (MPa)	1-20	5-70	58-95	-	1-80

It is further possible to compare the variation in the volume of the MOFs using the different methods (Table 1). In both MIL-53 systems, equivalent volumes are observed whether silicone oil or mercury are used as pressurization media. One could expect a maximum volume variation of 35% if one considers the variation in crystallographic volumes (unit cell volume of the LP form ≈ 1424 Å^3, and of the NP form ≈ 920 Å^3 for MIL-53(Al)). These are equally similar to those observed previously[23,29]. In the case of MIL-53(Cr), whilst the transition pressures are in good agreement with previous results [18] the MOF variation volume is smaller (0.2 mL g^{-1}) than 0.25 mL g^{-1} obtained by *Beurroies et al.*[18] with mercury porosimetry. This difference is certainly due to the sample quality or activation.

Previous studies with MIL-47(V) using mercury as a pressure medium, show a volume variation of 0.45 mL g^{-1} and a transition pressure for the compression in the range 85-125 MPa [24]. Whilst the pressure range compares well with what is observed here with silicone oil, the variation in the volume observed is lower which we again attribute to differences in sample quality.

The energies measured during the compression and decompression are reported in Figure 4. The data are reported

per mass. For all the MOFs studied, the compression is accompanied by an exothermal effect, whilst the decompression is endothermic. Indeed, in all of our current work, this is the case. The heats measured before and after the transition are null within experimental error. It shows that the heat of compressibility of the NP and LP forms are small.

At this point, it is interesting to compare this energetic behaviour with alternative mechanical energy systems using water intrusion into hydrophobic porous media. Here, water intrusion can be accompanied by an exothermic effect with the siliceous form of the zeolite chabazite,[26] or with hydrophobic mesoporous silica[28]. However, with silicalite-1 [26] or ZIF-8 [27] an endothermic effect is observed with water intrusion. This endothermal effect is predicted by thermodynamics when wetting is reversible[41].

In the present case, we consider that there is no, or negligible, pore filling by the silicone oil. Thus, for flexible MOF materials, the competition between two energetic contributions, one due to the deformation of the bond angles and the other due to the distance between ligands, stabilizes one of the structural forms of the material (LP or NP)[18]. Considering these results, it is shown that structural transition from LP to NP was exothermic, while the transition from NP to LP was endothermic. As a consequence, MOF materials store mechanical energy and dissipate thermal energy, whereas, heterogeneous lyophobic systems with reversible intrusion-extrusion, store mechanical and thermal energy. This latter behaviour is interesting because it should prevent heating when the material is submitted to successive cycles.

The mechanical work (W) and measured energies (Q) are reported in Table 2. From these values it is possible to calculate the change in internal energy (U) during compression or decompression as well as the variation in internal energy during each cycle. With the exception of MIL-47(V), the heat of compression is in the same range as the mechanical work.

The mechanical work obtained for MIL-53(Al) is about 7.8 J g^{-1} during the first compression, then, it stabilizes around 6.0 J g^{-1} for the next three cycles. These results are in good agreement with the value previously reported of 6.6 J g^{-1} by mercury porosimetry [23]. Among the three MOFs studied here, this sample is the only one which provides a heat energy higher than the work energy, resulting in a negative compression internal energy (ΔU$_{comp.}$) about -2.5 J g^{-1} and a positive decompression internal energy (ΔU$_{decomp.}$) around 3.0 J g^{-1}. Again these observations correspond to those previously reported[29].

The compression work energy measured for MIL-53(Cr) stays constant during the four cycles at approximately 9.0 J g^{-1}, which is lower than that previously reported (~14 J g^{-1}). [18] This is simply a result of the lower variation in volume observed for the sample studied here.

In the case of MIL-47(V), *Yot et al.*[24] reported a mechanical compression work of 32.9 J g^{-1} and a mechanical decompression work of -19.5 J g^{-1} upon mercury porosimetry up to 350 MPa. As observed in Table 2, the silicone oil system leads to values of 34 J g^{-1} and -23 J g^{-1} for compression and

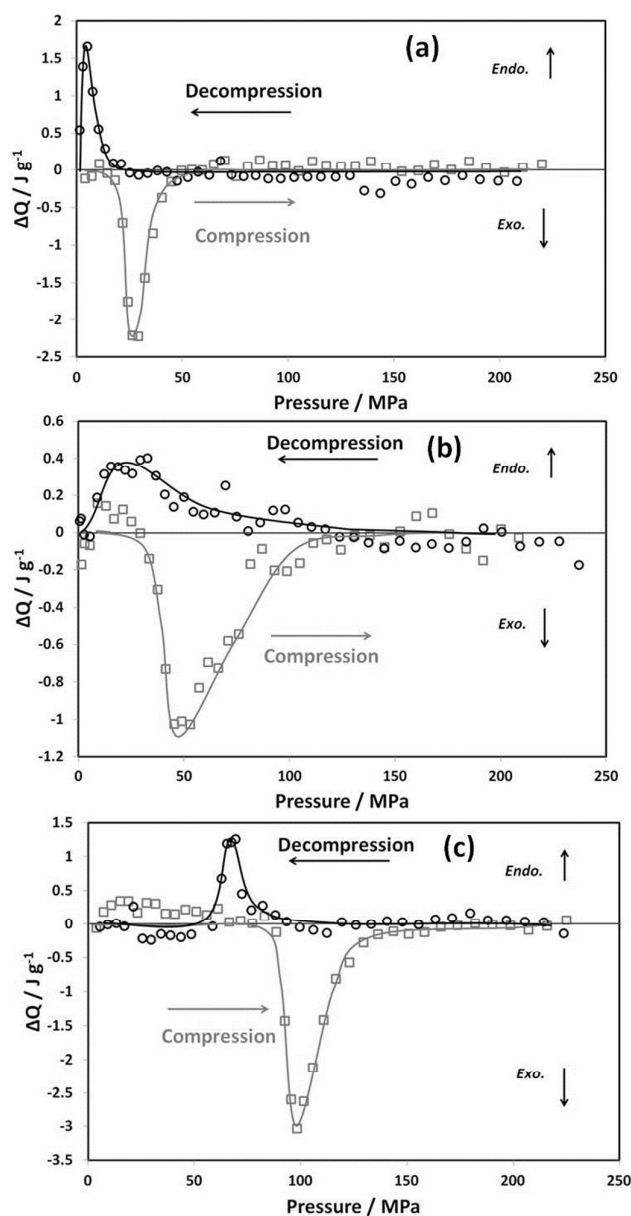decompression respectively which are in good agreement with the reported values.

Fig. 4 Heat of compression and decompression as a function of the applied oil pressure for MIL-53(Al) (a), MIL-53(Cr) (b) and MIL-47(V) (c) at 298K during a cycle of compression/decompression.

It is possible to evaluate the overall heating of the samples during each cycle, i.e. ($Q_{comp.}$ + $Q_{decomp.}$). For the MIL-53 samples, this can be evaluated in the range -4 to -5 J g^{-1} per cycle, whereas this value reaches -8 to -10 J g^{-1} cycle^{-1} for MIL-47(V). This can be significant as in a real device, without effective heat management, an increase in temperature of several °C per cycle could occur.

When considering the change in internal energy for each cycle, a totally reversible process should give a value of zero. For the two MIL-53 samples, this is more or less the case when one

takes into consideration the experimental errors. However, for the MIL-47(V) system, a significant difference is observed. It may be possible to attribute this to a slow decrease in the work of compression with each cycle from 35.2 J g-1 to 33.1 J g-1, which could be due to a gradual degradation of the structure under the experimental conditions, this solid being knwon to be less stable than the MIL-53 counterparts

Structural transition induced by temperature at constant pressure

Fig. 5 represents the heat flow as a function of the temperature for the MIL-53(Cr)-Br sample under helium flow when heated at 5°Cmin^{-1} and 10°Cmin^{-1}.
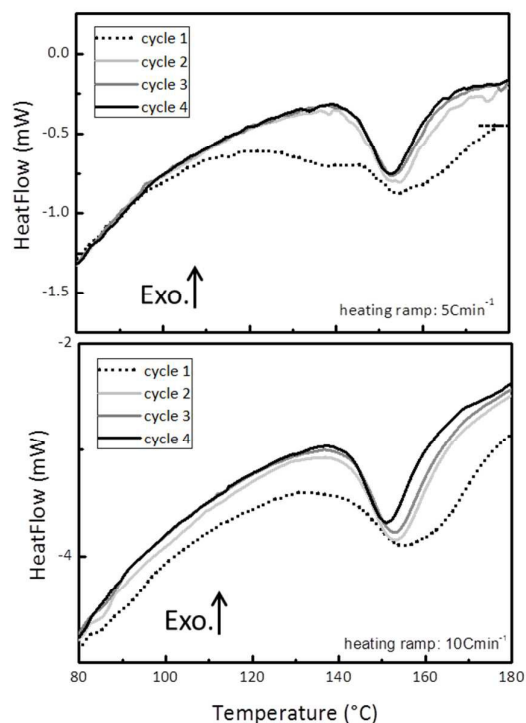

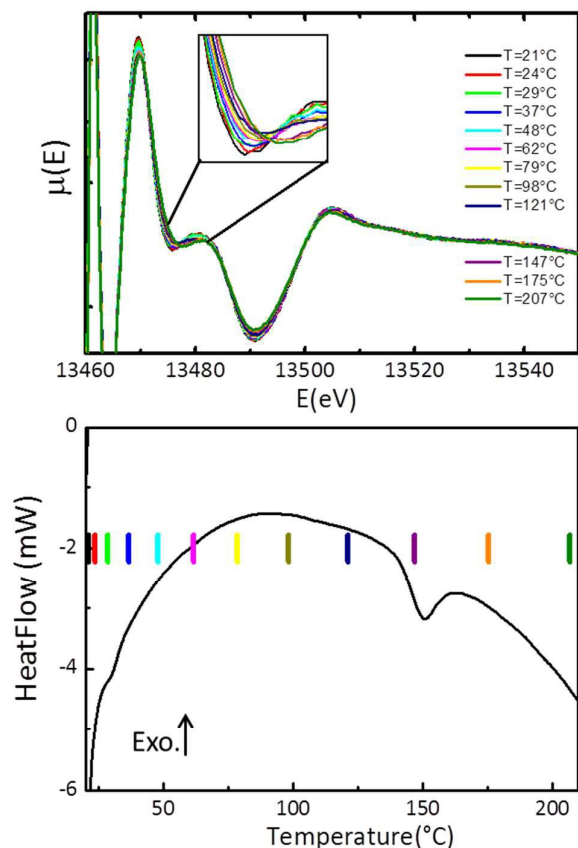**Fig. 5** DSC recording obtained at two different heating rates for MIL-53(Cr)-Br for successive cycles.

An endothermic peak is observed around 150°C and its width clearly decreases between the first cycle and the next ones. As previously explained, the sample is not activated prior to the DSC experiment. This means that, in its initial state, the sample contains residual water and has a NP structure. Thus during the first heating cycle two endothermic phenomena occur: water desorption and pore opening, which may explain the larger thermal effect.

During the following cycles, one may expect that only the structural NP→LP transition is observed. This assumption is confirmed by the XAS measurements. Indeed, as seen in Fig. 6, simultaneously to the transition observed by DSC, clear modifications in the XAS signal are evidenced. Those changes occur in the first 50eV after the absorption edge, the spectra are very sensitive to changes in the electronic structure around the absorbing atom. These changes are most probably related to a deviation in the local symmetry. Since the Br atoms are
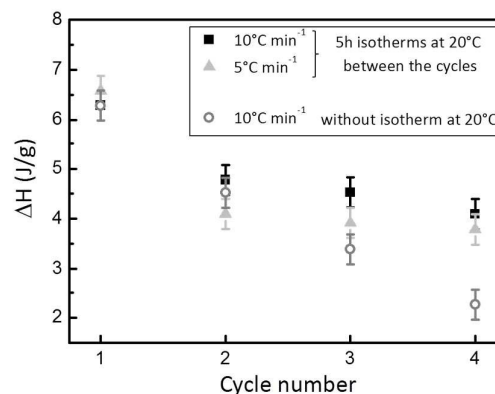
ARTICLE

probed, this indicates that the pore opening is a collective mechanism which includes also changes in the periphery of the structure. A detailed structure analysis will be published elsewhere.

Fig. 6 (a) XAS spectra measured using the DSC-XAS setup for different temperatures. Note that to ensure legibility only every second spectrum is presented. (b) DSC recording performed at 10°C min⁻¹ and acquired simultaneously to the XAS spectra. The vertical markers correspond to the temperature at which the XAS signal were acquired (colour online)

Interestingly, the magnitude of the transition slowly decreases with an increase in the number of cycles (Fig. 7). This could be related (i) to kinetics: the transition LP→NP transition is slower that the NP→LP or (ii) to sample degradation at high temperature. In order to rule on those points, the enthalpy values are calculated for different heating programs and the obtained values are given in Fig.7. They are also compared to the renormalized enthalpy values obtained during the DSC-XAS experiment for which there was no isotherm step at ambient temperature. It is worth noting that, whatever the heating program, the enthalpy values slightly decrease as the number of cycles increases. The decay is faster when the cycles are performed without any isotherm step at ambient temperature. This suggests that the kinetics of the LP→NP transition are slower than the ones related to pore opening. One may note that the enthalpy values obtained at 10°C min⁻¹ are slightly

lower than the ones obtained at 5°C min⁻¹. This may indicate that the sample slowly degrades at high temperature since lower is the heating rate, longer the sample remains at high temperature.

Fig. 7 Enthalpy variation associated to the NP→LP transition as a function of the cycle number for MIL-53(Cr)-Br obtained under different heating programs.

Although the obtained enthalpy variations for the NP→LP transition cannot be compared to the corresponding internal energy variation since they were obtained at different temperatures, one may however observe that they are in the same range of around a few Joules per gram.

Conclusions

In summary, this thermodynamic study of MOFs describes how (i) to measure the heat and mechanical work during the structural transition between the LP form and the NP form at constant temperature enabling calculation of the internal energy and (ii) to determine the enthalpy of the transition under the influence of temperature at constant pressure. It is shown that these values are in the same range for the MIL-53(Al or Cr) series whereas larger energy variations are obtained for the MIL-47 sample. These results are of fundamental importance to determine the performances and the possible heating of these materials as dampers in practical applications.

From a practical point of view, the MIL-53(Al) and MIL-53(Cr) seem to possess equivalent performances in both heat and mechanical work. Nevertheless, they differ by their transition pressure which is higher for MIL-53(Cr) than for MIL-53(Al) (≈55 MPa versus ≈30 MPa). Otherwise, the MIL-47(V) outperforms the mechanical energy storage capacity of other MOFs which makes it a promising candidate for damper applications, despite a higher heating. However, its small loss of mechanical work capacity during the first three cycles may reveal degradation problems that should be confirmed in future studies. On the other hand, MIL-53 (Cr)-Br may not be used as damper at around ambient temperature. However its

property of opening under the influence of temperature could be applied to a use as actuator.

Table 2 Measured mechanical work and energy obtained for the compression and decompression cycles of samples and calculated internal energy changes associated with each step.

Cycle	MIL-53(Al)				MIL-53(Cr)				MIL-47(V)		
	1	2	3	4	1	2	3	4	1	2	3
$W_{comp.}$ (J g^{-1})	7.8	6.3	5.9	5.9	9.5	9.4	8.7	9.2	35.2	33.9	33.1
$Q_{comp.}$ (J g^{-1})	-9.9	-9.4	-8.7	-8.2	-9.1	-8.1	-7.8	-8.3	-15.6	-13.0	-12.9
$\Delta U_{comp.}$ (J g^{-1})	-2.1	-3.1	-2.8	-2.3	0.4	1.3	0.9	0.9	19.6	20.9	20.2
$W_{decomp.}$ (J g^{-1})	-	-1.7	-2.0	-2.1	-5.1	-5.4	-5.5	-5.0	-23.8	-22.0	-22.9
$Q_{decomp.}$ (J g^{-1})	-	5.7	4.5	4.9	4.1	4.5	4.7	4.7	5.2	4.8	4.9
$\Delta U_{decomp.}$ (J g^{-1})	-	4.0	2.5	2.8	-1.0	-0.9	-0.8	-0.3	-18.6	-17.2	-18.0
ΔU_{cycle} (J g^{-1})	-	0.9	-0.3	0.5	-0.6	0.3	0.1	0.6	1.0	3.7	2.2

Notes and references

1   J.-Q. Zhang, Z.-Z. Peng, L. Zhang and Y. Zhang, *Proceedings of the World Congress on Engineering*, 2013, **Vol. III**, WCE 2013, july 3 – 5 London, U. K .
2   C. V. Suciu, T. Iwatsubo, and S. Deki, *J. of coll. and inter. sci.*, 2003, **259**, 62-80.
3   S. K. Jha, *J. of Sound and Vibr.*, 1976, **47**, 543-558.
4   C. V. Suciu, *Proceedings of ISMA2010*, 2010, International Conference on Noise and Vibration Engineering (ISMA)/Conference of USD, Leuven, BELGIUM, 4233-4245.
5   B. Lefevre, A.Saugey, J. L. Barrat, L. Bocquet, E. Charlaix, P. F. Gobin and G. Vigier, *Coll. Surf. A*, 2004, **241**, 265-272.
6   C. V. Suciu and K. Yaguchi, *Exp. Mechanics*, 2009, **49**, 383-393.
7   Ya. Grosu, O. Ievtushenko, V. Eroshenko, J. M. Nedelec and J. P. E. Grolier, *Coll. Surf. A*, 2014, **441**, 54
8   Y. Grosu, V. Eroshenko, J. M. Nedelec and J. P. E. Grolier, *Phys. Chem. Chem. Phys.*, 2015, **17**, 1572.
9   L. Tzanis, H. Nouali, T. J. Daou, M. Soulard and J. Patarin, *Mater. Let.*, 2014, **115**, 229-232.
10 I. Khay, L. Tzanis, T. J. Daou, H. Nouali, A. Ryzhikov and J. Patarin, *Phys. Chem. Chem. Phys.*, 2013, **15**, 20320-20325.
11 M. A. Saada, S. Rigolet, J.-L. Paillaud, N. Bats, M. Soulard and J. Patarin, *J. Phys. Chem. C*, 2010, **114**, 11650-11658.
12 T. Karbowiak, C. Paulin, B. Ballandras, G. Weber, J.-P. Bellat *J. Am. Chem. Soc.*, 2009, **131**, 9898–9899.
13 G. Férey, *Chem. Soc. Rev.* 2008, **37**, 191-214.
14 G. Férey, C. Serre, T. Devic, G. Maurin, H. Jobic, P. L. Llewellyn, G. De Weireld, A. Vimont, M. Daturi and J. S. Chang, *Chem. Soc. Rev.*, 2011, **40**, 550-562.
15 J. Gascon, A. Corma, F. Kapteijn, and F. Llabrés i Xamena, *ACS Catal.*, 2014, **4**, 361-378.
16 P. Horcajada, R. Gref, T. Baati, P. K. Allan, G. Maurin, P. Couvreur, G. Férey, R. E. Morris and C. Serre, *Chem. Rev.*, 2011, **112**, 1232-1268
17 G. Ortiz, G. Chaplais, J.-L. Paillaud, H. Nouali, J. Patarin, J. Raya, and C. Marichal, *J. Phys. Chem. C*, 2014, **118**, 22021–22029
18 I. Beurroies, M. Boulhout, P. L. Llewellyn, B. Kuchta, G. Férey, C. Serre and R. Denoyel, *Angew. Chem., Int. Ed.*, 2010, **49**, 7526-7529.
19 T. Loiseau, C. Serre, C. Huguenard, G. Fink, F. Taulelle, M. Henry, T. Bataille and G. Férey, *Chem. Eur. J.*, 2004, **10**, 1373-
20 C. Serre, F. Millange, C. Thouvenot, M. Noguès, G. Marsolier, D. Louër and G. Férey, *J. Am. Chem. Soc.*, 2002, **124**, 13519-13526.
21 K. Barthelet, J. Marrot, D. Riou and G. Férey, *Angew. Chem. Int. Ed.*, 2002, **41**, 281-284.
22 E. Alvarez, N. Guillou, C. Martineau, B. Bueken, B. Van de Voorde, C. Le Guillouzer, P. Fabry, F. Nouar, F. Taulelle, D. de Vos, J.-S. Chang, K. H. Cho, N. Ramsahye, T. Devic, M. Daturi, G. Maurin and C. Serre, *Angew. Chem.*, 2015, **127**,1-6.
23 P. G. Yot, Z. Boudene, J. Macia, D. Granier, L. Vanduyfhuys, T. Verstraelen, V. Van Speybroeck, T. Devic, C. Serre, G. Férey, N. Stock, G. Maurin, *Chem. Comm.*, 2014, **50**, 9462-9464.
24 P. G. Yot, Q. Ma, J. Haines, Q. Yang, A. Ghoufi, T. Devic, C. Serre, V. Dmitriec, G. Férey, C. Zhong and G. Maurin, *Chem. Sci.*, 2012, **3**, 1100-1104.
25 T. Karbowiak, C. Paulin and J.-P. Bellat, *Microp. And Masop. Mater.*, 2010, **134**, 8-15.
26 T. Karbowiak, G. Weber and J.-P. Bellat, *Langmuir*, 2014, **30**, 213-219.
27 Ya. Grosu, G. Renaudin, V. Eroshenko, J.- M. Nedelec and J.-P. E. Grolier, *Nanoscale*, 2015, **7**, 8803–8810.
28 F. Gomez, R. Denoyel and J. Rouquerol, *Langmuir*, 2000, 16, 4374-4379.
29 J. Rodriguez, I. Beurroies, T. Loiseau, R. Denoyel and P. L. Llewellyn, *Angew. Chem., Int. Ed.*, 2015, **54**, 4626-4630.
30 M. B. Dogruoz, E. L. Wang, F. Gordaninejad, A, J. Stipanovic, *J. of Intel. Mater. Syst. and Struc.*, 2003, **14**, 79-86.
31 D. Bartterbee and D. Sims, *J. of Intel. Mater. Syst. And Struct.*, 2009, **20**, 297-309.

32 P. S. Els, B. Grobbelaar, *J. of Terramechanics*, 1999, **36**, 197-205.

33 P. Serra-Crespo, A. Dikhtiarenko, E. Stavitski, J. Juan-Alcañiz, F. Kapteijn, F.-X. Coudert and J. Gascon, *CrystEngComm*, 2015, **17**, 276-280.

34 K. W. Chapman, G. J. Halder and P. J. Chapus, *J. Amer. Chem. Soc.*, 2009, **131**, 17546-17547.

35 E. C. Spencer, R. J. Angel, N. L. Ross, B. E. Hanson, J. A. K. Howard, *J. Amer. Chem. Soc.*, 2009, **131**, 4022-4026.

36 C. Serre F. Millange , C. Thouvenot , M. Noguès , G. Marsolier, D. Louër and G. Férey, *J. Am. Chem. Soc.*, 2002, **124**, 13519–13526.

37 T. Loiseau, C. Serre, C. Huguenard, G. Fink, F. Taulelle, M. Henry,T. Bataille and G. Férey, *Chem. Eur. J.* 2004, **10**, 1373-1382.

38 K. Barthelet, J. Marrot, D. Riou and G. Férey, *Angew. Chem. Int. Ed.* 2002, **41**, 281-284.

39 V. Guillerm, 2011, Synthèse, fonctionnalisation et propriétés d'adsorption de nouveaux solides hybrides poreux, PhD Thesis, Université de Versailles.

40 P. Zalden, G. Aquilanti, C. Prestipino, O. Mathon, B. André, M. Wuttig, M.-V. Coulet, *J. Synchrotron Rad.*, 2012, **19**, 806-813.

41 Eroshenko, V. A., *Proc. of Institution Mechanical Engineers Part D*, 2007*,* **221**, 285-300.

Dalton Transactions Accepted Manuscript